Title

Occupancy and Fractal Dimension Analyses of the Spatial Distribution of Cytotoxic (CD8+) T Cells Infiltrating the Tumor Microenvironment in Triple Negative Breast Cancer

Journal

Biophysical Reviews and Letters, 15(02)

ISSN

1793-0480

Authors

Wortman, Juliana C
He, Ting-Fang
Rosario, Anthony
et al.

Publication Date

2020-06-01

DOI

10.1142/s1793048020500022

Peer reviewed

Biophysical Reviews and Letters
Vol. 15, No. 2 (2020) 83–98

DOI: 10.1142/S1793048020500022

World Scientific
www.worldscientific.com

Occupancy and Fractal Dimension Analyses of the Spatial Distribution of Cytotoxic (CD8$^+$) T Cells Infiltrating the Tumor Microenvironment in Triple Negative Breast Cancer

Juliana C. Wortman[*], Ting-Fang He[†], Anthony Rosario[†], Roger Wang[†], Daniel Schmolze[‡], Yuan Yuan[§], Susan E. Yost[§], Xuefei Li[¶], Herbert Levine[¶], Gurinder Atwal[‖], Peter Lee[†] and Clare C. Yu[*,**]

[*]*Department of Physics and Astronomy*
University of California, Irvine 92697, CA

[†]*Cancer Immunotherapeutics & Tumor Immunology*
City of Hope Comprehensive Cancer Center and Beckman Research Institute
1500 East Duarte Road, Duarte 91010, CA

[‡]*Department of Pathology*
City of Hope Comprehensive Cancer Center and Beckman Research Institute
1500 East Duarte Road, Duarte 91010, CA

[§]*Department of Medical Oncology and Molecular Therapeutics*
City of Hope Comprehensive Cancer Center and Beckman Research Institute
1500 East Duarte Road, Duarte 91010, CA

[¶]*Department of Bioengineering and the Center for Theoretical Biological Physics*
Rice University, Houston 77030, TX

[‖]*Cold Spring Harbor Laboratory, Cold Spring Harbor, NY 11724*
[**]*cyu@uci.edu*

Received 6 February 2020
Revised 1 April 2020
Accepted 6 April 2020
Published 25 June 2020

Favorable outcomes have been associated with high densities of tumor infiltrating lymphocytes (TILs) such as cytotoxic (CD8$^+$) T cells. However, the clinical significance of the spatial distribution of TILs is less well understood. We have developed novel statistical techniques to characterize the spatial distribution of TILs at various length scales. These include a box counting method that we call "occupancy" and novel applications of fractal dimensions. We apply these techniques to the spatial distribution of CD8$^+$ T cells in the tumor microenvironment of tissue resected from 35 triple negative breast cancer patients. We find that there is a distinct difference in the spatial distribution of CD8$^+$ T cells between good clinical outcome (no recurrence within at least 5 years of diagnosis) and poor clinical outcome (recurrence within 3 years of diagnosis). The statistical significance of the difference between good and poor outcome in the occupancy, fractal dimension (FD), and FD difference of CD8$^+$ T cells is comparable to that of the CD8$^+$ T cell density. Even when we randomly exclude some of the cells so that the images have the same cell density, we still find that the fractal dimension at short length scales is correlated with cancer recurrence, implying that the actual spatial distribution of CD8$^+$ cells,

**Corresponding author.

and not just the $CD8^+$ cell density, is associated with clinical outcome. The occupancy and FD difference indicate that the $CD8^+$ T cells are more spatially dispersed in good outcome and more aggregated in poor outcome. We discuss possible interpretations.

Keywords: Triple negative breast cancer; tumor infiltrating lymphocytes; T cells; tumor microenvironment; spatial distribution; fractal dimension.

1. Introduction

Note: Some of the material in this paper is in our archived papers, Refs. 1 and 2, where more details and results can be found.

Tumors are heterogeneous, consisting of numerous components including cancer cells, collagen fibers, blood vessels, lymph vessels, fibroblasts, and various types of immune cells. The cancer cells cluster to form cancer cell islands that are typically hundreds of microns in diameter. These cancer cell islands are surrounded by stroma where most of the immune cells, such as lymphocytes, reside. The two main types of lymphocytes are B cells, which perform a variety of functions such as making antibodies, and T cells. $CD8^+$ T cells are cytotoxic or "killer" T cells.

Numerous studies have found that high densities of tumor infiltrating lymphocytes (TILs) correlate with favorable clinical outcomes.[3–5] For example, higher densities of $CD3^+$ and $CD8^+$ T cells were associated with a lower rate of recurrence in hepatocellular carcinoma.[6] In addition, immunotherapy is more effective when T cells infiltrate the tumor, e.g., a higher density of $CD8^+$ T cells in melanoma tumors is directly correlated with a better prognosis and clinical response to checkpoint inhibitors.[7]

However, analyzing only the density of immune cells neglects the heterogeneous distribution of immune cells in the tumor tissue. This heterogeneity could even skew density measurements by over/underestimating the density, depending on the location of the samples in the tissue. There are indications of the clinical relevance of the spatial distribution of T cells[8] and around[9] tumors. In this paper, we present novel ways to analyze the heterogeneity and spatial distribution of TILs to determine whether they provide additional information, beyond what is captured by the density alone.

There have been a number of efforts to quantify spatial heterogeneity of the tumor microenvironment based on comparing populations of cells.[10] For example, Saltz *et al.* used deep learning to identify 50×50 micron patches with a high density of TILs in digitized H&E stained images of 13 different tumor types from The Cancer Genome Atlas (TCGA).[8] They used a technique known as affinity propagation to group the patches into clusters, and found that the number and spatial extent of the clusters is correlated with clinical outcome. However, there is no unique way to define which patch belongs to which cluster. In addition, the typical size of the clusters depends on an input parameter. In another example, the Morisita–Horn index was used to quantify the spatial colocalization of tumor and immune cells, and it was found that significant colocalization was associated with a higher disease-specific

survival in Her2-positive breast cancers.[10,11] The Getis–Ord analysis[12] was used to locate immune hotspots where the clustering of immune cells was significantly above background. A combined immune-cancer hotspot score was found to be associated with good prognosis in ER-negative breast cancer.[13] A quantitative measure of the infiltration of immune cells into a tumor is the intratumor lymphocyte ratio (ITLR) which is defined as the ratio of the number of intratumor lymphocytes to the total number of cancer cells in a histological sample.[14] A high ITLR was found to be associated with good disease specific survival in ER-negative/Her2-negative breast cancer.[14,15]

Natrajan *et al.*[16] quantified the spatial heterogeneity in breast tumors with regard to cancer cells, lymphocytes and stromal cells by calculating the Shannon entropy in different regions of the tumor and using Gaussian mixture models to fit the distribution of Shannon entropies. Their ecosystem diversity index (EDI) was the number of Gaussians needed to fit the distribution. They found that high EDI values were associated with high micro-environmental diversity and poor prognosis. Somewhat ironically, with this measure, if most of the regions have high Shannon entropies such that a single Gaussian can be used to fit the distribution, then the EDI is low.

Fractal dimensions[17] have been used to characterize the irregular morphology of tumors[18–20] and vasculature[21,22] as well as subcellular structures such as mitochondria[23] and nuclei.[24] There are numerous ways to calculate fractal dimensions. In the box counting method, the number $N(L)$ of squares (each with area L^2) needed to cover the 2D image of, e.g., a tumor, is proportional to L^{-d}, where d is the fractal dimension in the limit that L goes to zero (or a very small value). More irregular shapes correspond to higher fractal dimensions and poorer prognoses.[18,19]

Assuming that the structure of tumor tissue is reflected in the arrangement of cancer cell nuclei, Waliszewski *et al.* calculated several different fractal dimensions as well as the Shannon entropy and lacunarity to characterize the spatial distribution of cancer cell nuclei in prostate tumor tissue and compared the results to the corresponding Gleason scores in an attempt to find a more objective way to classify prostate tumor tissue.[25,26]

Unlike these previous approaches that quantified the spatial distribution at a single length scale, our techniques use coarse graining to characterize the spatial distribution at different length scales. As an example, we analyze the spatial distribution of T cells in images of tumor tissue from a small group of patients with triple negative breast cancer (TNBC). Our results indicate that T cells tend to be more spatially dispersed in cases where TNBC does not recur and to be more clustered when TNBC does recur.

2. Methods

Occupancy[1,2]: The goal of quantifying the spatial distribution of some entity is to map it to a scalar (number). In our case, we start with 2D images of tissue samples with various types of cells stained with chromophores. We then overlay the image with a grid of squares as in Fig. 1(a). Each square has an area of L^2. For each square,

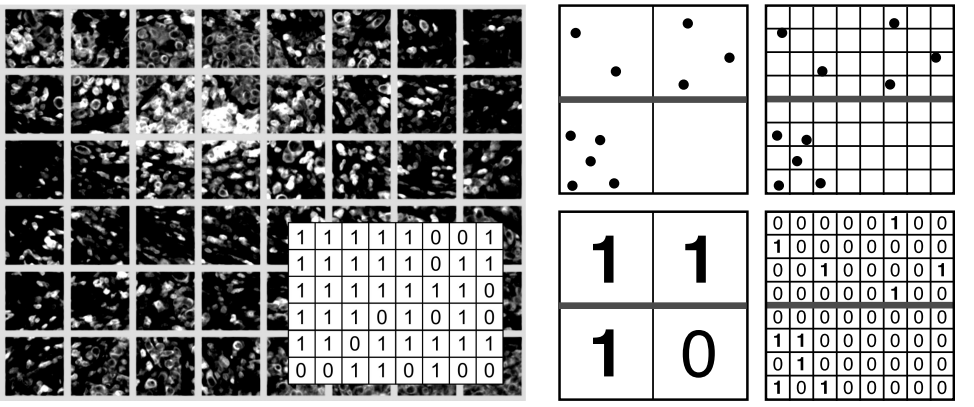

(a) (b)

Fig. 1. (a) Diagrams illustrating occupancy analysis. (a) Grid of squares superimposed on tissue. (a, inset) Grid of squares with 0's and 1's indicating the answer to a yes–no question. (b) Cartoon illustrating how FD difference can determine the spatial dispersion of cells. The upper halves (above the thick black lines) of the two images show points that are spread out while the lower halves show clustered points. At long length scales (big boxes) the FD is 2 in the upper half but not in the lower half. At small length scales (small boxes), both halves have the same number of boxes with points and hence the same fractal dimension. Thus, the difference in FD between large and small length scales is greater for points that are more spread out.[1,2]

we ask a binary (yes–no) question, e.g., "Is there at least one $CD8^+$ T cell in the square?" If the answer is yes, we assign a 1 to that square. If the answer is no, we assign a 0 to the square (see Fig. 1(b)). The occupancy p is the fraction of squares with 1's, i.e., it is an estimate of the probability that a square will have a 1. To characterize the spatial distribution at different length scales, we varied the size of the squares in the grid and computed the occupancy as a function of L, the length of one side of a square. We can calculate the area under the curve (AUC) of occupancy versus L as a way to characterize the curve.

Fractal Dimension[1,2]: While there are a number of different ways to define the fractal dimension, we use a variation of the box counting method.[27] We again imagine overlaying the image with a grid of squares as described above, assigning a '1' (or '0') to the square if the answer to a binary question is yes (or 'no'). Let each square have size $L \times L$. The number $n(L)$ of squares with '1' will be proportional to $(1/L^d)$, where d is an exponent less than or equal to the dimension of the image, i.e., 2. In fact, d is one type of fractal dimension. If the system is self-similar and fractal over a range of length scales L, $n(L)$ should follow a power law: $n(L) \sim (1/L^d)$ and the exponent d should be independent of L. So we plot $\log [n(L)]$ versus $\log[A/L]$, where A is a constant, and use linear regression to fit a least squares line through the points. The fractal dimension x is defined to be the slope of the line: $x = -d[\log n(L)]/d[\log L]$. We use a different variable, x, rather than d in the event that $n(L)$ does not follow a simple power law as L is varied. The fractal dimension is

found for each patient and then averaged over patients with a given clinical outcome, i.e., good clinical outcome, poor clinical outcome and normal tissue.

Relation of Occupancy and Fractal Dimension[2]: There is a simple relation between the dependence of occupancy on L and fractal dimension d. Suppose the total number $N(L)$ of squares covering the image of the tissue goes as $(1/L^D)$. Then if $n(L) \sim (1/L^d)$, the occupancy $p = n(L)/N(L) \sim L^{D-d}$. Note that D need not be equal to 2 since the image of the tissue may be irregular or there may be regions that were not imaged.

Fractal Dimension Difference[1,2]: A way to determine whether cells are clustered or spread out is to calculate the difference Δs in fractal dimension between large and small length scales: $\Delta s = s_{\text{Large}} - s_{\text{small}}$, where s_{Large} is the fractal dimension at large length scales and s_{small} is the fractal dimension at small length scales. The small and large length scales should roughly bracket the typical, or median, nearest neighbor distance between cells of the same type, e.g., $CD8^+$ T cells. In all the cases we examined, $\Delta s > 0$. If Δs is large, it means that the cells are more dispersed, i.e., more spatially spread out because they appear more two-dimensional at large length scales and more zero-dimensional (point-like) at small length scales (see Fig. 1(b)). If $\Delta s = 0$, the fractal dimension does not change with length scale and the system is self-similar, i.e., fractal. If Δs is small, then the system is closer to being fractal and the cells are more aggregated. In this paper, the large length scale range is 200–600 microns and the small length scale range is 10–40 microns.

3. Breast Cancer Tissue Samples

We obtained primary tumor tissue resected from 37 triple negative breast cancer patients[1,2]: 24 patients had a good clinical outcome (no recurrence within 5 years) and 13 patients had poor clinical outcome (recurrence within 3 years). As a control, we also analyzed the normal breast tissue from 9 patients who underwent reduction mammoplasty (breast reduction surgery). None of the patients had received chemotherapy or radiation at the time of resection. The baseline patient information is presented in Table 1.

Tissue preparation[1]: Specimens were identified through an IRB-approved protocol via the City of Hope (COH) Biospecimen Repository which is funded in part by the National Cancer Institute. Other investigators may have received specimens from the same patients. Samples from patients diagnosed with triple negative breast cancer and treated at COH from January 1, 1994 to March 4, 2015 were retrieved. Eligible patients had the following features: stages I–III breast cancer; at least one tumor biospecimen was available from the initial surgical resection or biopsy; clinical outcome data was available for identification of relapse free survival; no prior treatment at the time of surgical biopsy. Archived formalin-fixed paraffin-embedded (FFPE) tumor tissues were sectioned (i.e., 3–5 microns per slide) and baked onto glass microscope slides. Immunostaining was performed with anti-pan cytokeratin (clone AE1/AE3, Dako), anti-CD8 (clone SP16, Biocare), and anti-CD20

Table 1. Baseline patient information. In the TNM classification, T denotes tumor burden, N denotes lymph node classification, and M denotes the metastasis status. No patients were known to have any metastasis at the time of their initial surgery.

	Good outcome	Poor outcome	Normal tissue
Number of patients	24	13	9
Mean Age	55	58	24
Age Range	27–76	46–79	18–45
Stage I	5	7	
Stage II	17	6	
Stage III	2	0	
Stage IV	0	0	
T1	7	7	
T2	16	6	
T3	1	0	
N0	19	11	
N1	3	2	
N2	2	0	
M0	3	0	
M1	0	0	
MX	21	13	
Grade 1	0	0	
Grade 2	3	1	
Grade 3	21	12	
Mastectomy	15	2	
Breast conserving surgery	9	11	

(L26, Dako) antibodies using the Opal TSA (PerkinElmer). Samples were further counterstained with DAPI to visualize the nuclei of all cells. Prior to imaging, the tissue sections were coverslipped with ProLong® Gold Antifade mounting media (Cat. # P36930, Life Technologies). All the images were acquired using the Vectra 3.0 Automated Quantitative Pathology Imaging System (PerkinElmer). We used commercial (inForm Image Analysis Software, PerkinElmer and TIBCO Spotfire Software) and in-house custom developed software (R) and algorithms to, at a minimum, identify each cell, define its type (cancer or specific immune), and assign it Cartesian coordinates, allowing the image processing described below. Using an automated tissue segmenter algorithm built in inForm®, we further divided the images into areas of cancer islands and stroma based on anti-pan cytokeratin antibody staining.

Multispectral staining: The following cell phenotypes were identified on the same slide: cytotoxic (killer) T cells ($CD8^+$), B cells ($CD20^+$), epithelial/cancer cells (PanCK), or "other". The cells were also counterstained with DAPI to show the location of nuclei.

Regions of Interest[1]: A pathologist delineated tumor regions that were deemed representative of the entire tumor in terms of cellularity and the TIL distribution,

and that were free of artifacts such as tissue folding. Obvious large swaths of necrotic tumor were avoided, as were peri-tumoral lymphoid aggregates not in close proximity to the tumor cells. Given these constraints, regions were chosen to maximize tumor area.

Image Analysis[1]: We tiled each image with a grid of identical squares. We omitted squares that had no cells, since they lay outside the tissue. However, we included squares that were within the tissue but contained no cells of interest. The length L of one side of a square varies from 10 μm to 600 μm. To determine if a square received a '1' or a '0', we asked a yes-no question, e.g., "Is there at least one $CD8^+$ T cell in this square?" We processed the data using the R packages "spatstat" for point patterns and "EBImage" for raster images.[28,29]

For comparison, we calculated the occupancy and fractal dimension of a random (Poisson) distribution of points with uniform density.[1]

To ascertain whether a quantity, such as $CD8^+$ T cell density, is clinically significant, we calculated the p-value under the null hypothesis and receiver operating characteristic (ROC) area under the curve (AUC), both standard statistical measures of a binary classifier.[1,30] In our case, for the binary classifier, we assumed the clinical outcome was either good or poor. Typically, a p-value less than 0.05 indicates that the result is statistically significant. The ROC curve is a parametric curve where the parameter is a cutoff value for the quantity of interest, e.g., $CD8^+$ T cell density, the x-axis is the false positive rate, and the y-axis is the true positive rate. The ROC AUC varies from 0 to 1. High ROC AUC values indicate that the quantity is a good predictor of clinical outcome. A ROC AUC value of 0.5 means the quantity does no better than random chance.

4. Results

Occupancy, fractal dimension and FD difference of $CD8^+$ T cells are associated with clinical outcome.[1,2] Figure 2 is a plot of the average occupancy for $CD8^+$ T cells, i.e., the fraction of boxes with 1's, as a function of the square size L. The occupancy for points randomly placed according to a Poisson distribution is shown as a solid black line in Fig. 2; clearly, T cells are not randomly distributed. The difference between good and poor clinical outcome reflects, to some extent, the difference in T cell density. The average $CD8^+$ T cell density in the tumor is higher in patients with good outcome ($4.5 \times 10^4/\text{cm}^2$) than poor outcome ($2.1 \times 10^4/\text{cm}^2$). The flattening of the curves at large square sizes is reminiscent of scale invariance, suggesting the use of fractal dimensions.

The slope of the plot of $\ln(n(L))$ versus $\ln(1/L)$ in Fig. 3(a) gives the fractal dimension (FD).[1,2] Larger fractal dimensions, especially those close to two, correspond to more spatially uniform distributions of cells. Randomly placed points (Poisson distribution) are two-dimensional at large length scales as expected. For T cells at long length scales (where the data can be fit to a straight line) good outcome has a larger fractal dimension and therefore is more area-filling than poor outcome

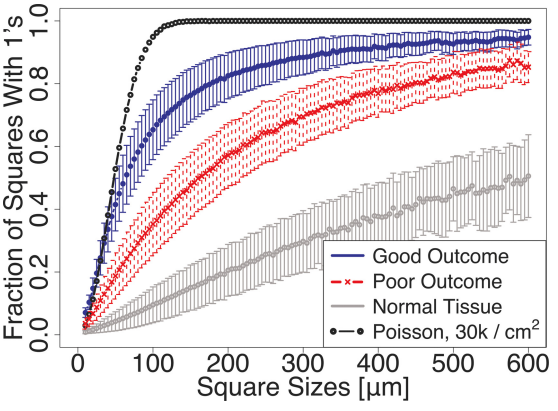

Fig. 2. (Color online) Plot of CD8$^+$ T cell occupancy versus square size for good clinical outcome (blue, solid), poor clinical outcome (red, dashed) and points randomly distributed according to a uniform Poisson process with a density of 3×10^4 points/cm^2 (solid black line). The error bars indicate 95% confidence intervals.[1,2]

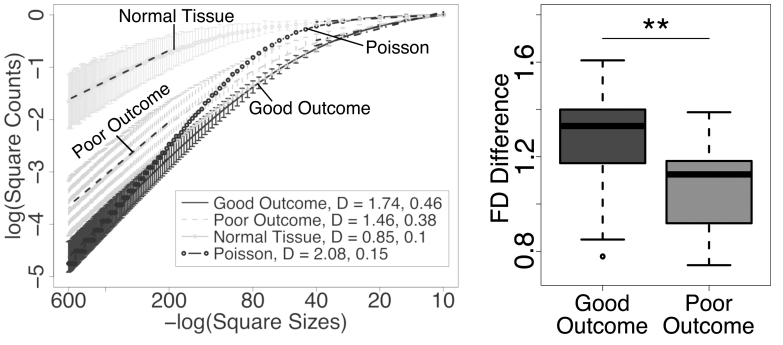

(a) (b)

Fig. 3. (a) Log–log plot of the number of squares with at least one CD8$^+$ T cell versus the inverse box size in microns. (Logarithms are base e.) At long length scales (200–600 microns on the left side of plot), the mean fractal dimension x (slope) is 1.74 for good outcome (dark, solid), 1.46 for poor outcome (light, dashed), 0.85 for normal tissue (light, solid) and 2.08 for Poisson (black). The p-value for good versus poor outcome is 3×10^{-4} at long length scales. At short length scales (10–40 microns on the right side of the plot), the mean fractal dimension is 0.46 for good outcome, 0.38 for poor outcome, 0.1 for normal tissue and 0.15 for Poisson. The p-value for good versus poor outcome is 0.09 at short length scales. Black dashed lines show the least squares linear regression fit at long and short length scales. Because different images had different numbers of squares containing tissue (cells of any type), for each image, we normalized the number $n(L)$ of boxes with 1's by the total number $N(L)$ of boxes with cells in computing the fractal dimension. Thus, the y-axis values are negative. The error bars correspond to 95% confidence intervals. The slope used to find the fractal dimension is from a least squares fit made using linear regression. This is true of all subsequent plots. (b) Box and Whisker plot showing that the median FD difference between large (200–600 microns) and small (10–40 microns) length scales for CD8$^+$ T cells is clinically significant ($p = 1.5 \times 10^{-5}$, ROC AUC = 0.88). The line in the middle of each box is plotted at the median, and the inferior and superior limits of the box correspond to the 25th and 75th percentiles, respectively. The whiskers correspond to the minimum and maximum values. Since the difference in median values is significant, the bar at the top is marked with two asterisks corresponding to $p < 0.01$.

which may be due to the higher $CD8^+$ T cell density in patients with a good outcome. The median FD difference between large (200–600 microns) and small length scales (10–40 microns) is larger for good outcome and clinically significant as shown in Fig. 3(b). This indicates that the $CD8^+$ T cells are more spatially dispersed for good outcome and more aggregated for poor outcome.

To determine whether the difference in fractal dimension and FD difference between good and poor clinical outcome is solely the result of the difference in cell density, we thinned the density by randomly eliminating $CD8^+$ T cells in the various images until the densities were the same value (2549 cells/cm^2) in all the tissue images.[1,2] Figure 4(a) is a log–log plot of the number of boxes with at least one $CD8^+$ T cell versus the logarithm of the inverse box size. With the same density, there is still a statistically significant difference between the fractal dimension of good and poor outcome patients at all length scales, indicating that the spatial distribution of the $CD8^+$ T cells is correlated with clinical outcome. At long length scales (200–600 microns), the thinned fractal dimension is slightly higher for poor

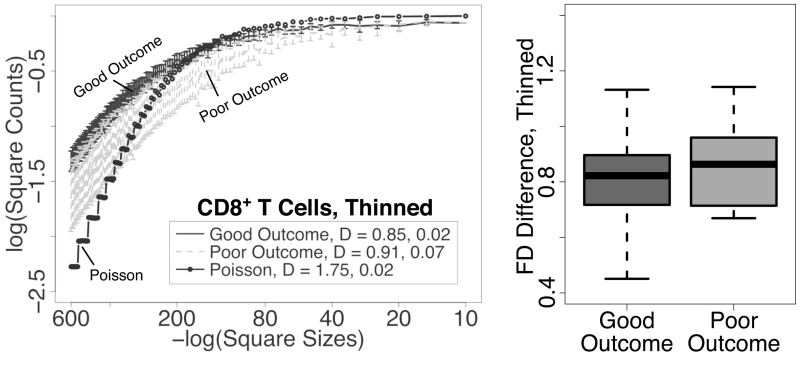

(a) (b)

Fig. 4. (a) Log–log plot of the number of squares with at least one $CD8^+$ T cell versus the inverse box size (in microns) for images where the T cell density has been reduced to 2,549 cells/cm^2 in each image. The fractal dimension x at large length scales (200–600 microns on the left side of the plot) is 1.75 for the Poisson distribution, 0.85 for good outcome, and 0.91 for poor outcome. The p-value for good versus poor outcome is 0.41 at long length scales. The fractal dimension at short length scales (10–40 microns) is 0.02 for Poisson, 0.02 for good outcome, and 0.07 for poor outcome. The p-value for good versus poor outcome is 0.035 for short length scales. At intermediate length scales (50 to 200 microns), the fractal dimension for Poisson is 0.22, and the fractal dimension for poor outcome is higher ($x = 0.33$) than for good outcome ($x = 0.18$), with a p-value of 1.6×10^{-3}. Black dashed lines show the least squares linear regression fit at long and short length scales. Because different images had different numbers of squares with tissue (cells of any type), for each image, we normalized the number $n(L)$ of boxes with 1's by the total number $N(L)$ of boxes with cells in computing the fractal dimension. Thus, the y-axis values are negative. The error bars correspond to 95% confidence intervals. (b) Box and whisker plot showing that the median FD difference between large (200–600 microns) and small (10–40 microns) length scales for thinned $CD8^+$ T cells is not clinically significant ($p = 0.83$, ROC AUC = 0.47). The line in the middle of each box is plotted at the median, and the inferior and superior limits of the box correspond to the 25th and 75th percentiles, respectively. The whiskers correspond to the minimum and maximum values.

outcome (0.91) than for good outcome (0.85). The fractal dimension of the thinned point patterns at short length scales between 10 and 40 microns is significantly higher for poor outcome ($x = 0.07$) than for good outcome ($x = 0.02$), with a p-value of 0.035 (see Fig. 4(a)). However, the median FD difference for thinned CD8$^+$ T cells is not clinically significant, indicating that the spatial dispersion of thinned CD8$^+$ T cells is not substantially different between good and poor outcome as shown in Fig. 4(b).

Fractal dimension and FD difference of CD8$^+$ T cells in cancer cell islands is clinically relevant.

While most CD8$^+$ T cells are found in the stroma, a few are located in cancer cell islands. The fractal dimension, as well as the FD difference, of CD8$^+$ T cells in cancer cell islands is relevant to clinical outcome (Fig. 5). In contrast, the fractal dimension

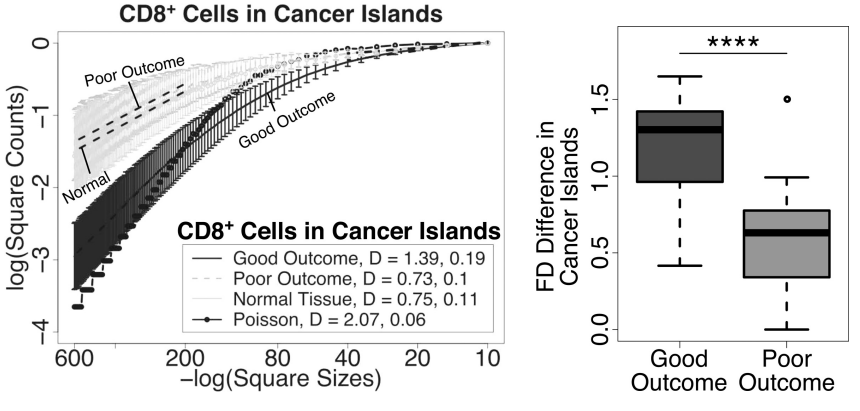

(a) (b)

Fig. 5. (a) Log–log plot of the number of squares with at least one CD8$^+$ T cell that is in a cancer cell island/epithelial tissue versus the inverse box size in microns. At long length scales (200–600 microns on the left side of plot), the mean fractal dimension x (slope) is 1.39 for good outcome (dark, solid), 0.73 for poor outcome (light, dashed), 0.75 for normal tissue (light) and 2.07 for Poisson (black). The p-value for good versus poor outcome is 1.1×10^{-5} at long length scales. At short length scales (10–40 microns), the mean fractal dimension x (slope) is 0.19 for good outcome (dark, solid), 0.10 for poor outcome (light, dashed), 0.11 for normal tissue (light, solid) and 0.06 for Poisson (black). The p-value for good versus poor outcome is 0.014 at short length scales. Black dashed lines show the least squares linear regression fit at long and short length scales. Because different images had different numbers of squares with tissue (cells of any type), for each image, we normalized the number $n(L)$ of boxes with 1's by the total number $N(L)$ of boxes with cells in computing the fractal dimension. Thus, the y-axis values are negative. The error bars correspond to 95% confidence intervals. (b) Box and whisker plot showing that the median FD difference between large (200–600 microns) and small (10–40 microns) length scales for CD8$^+$ T cells in cancer cell islands is clinically significant ($p = 1.5 \times 10^{-5}$, ROC AUC = 0.88). The line in the middle of each box is plotted at the median, and the inferior and superior limits of the box correspond to the 25th and 75th percentiles, respectively. The whiskers correspond to the minimum and maximum values. Since the difference in median values is significant, the bar at the top is marked with four asterisks corresponding to $p < 0.0001$.

and the FD difference of $CD8^+$ T cells in the stroma are not as strongly associated with outcome but are still statistically significant (see Table 2).

Fractal dimensions of cells (of all types) in cancer cell islands and the stroma do not explain the difference in fractal dimension of $CD8^+$ T cells in good and poor outcome.

The fractal dimension of the $CD8^+$ T cell distribution differs significantly between good and poor clinical outcome but this is not necessarily true for other types of cells. For example, the fractal dimension of the distribution of cells (of any type) occupying cancer cell islands is not significantly different between good and poor outcome as shown in Fig. 6(a). In the case of cells in stroma (Fig. 6(b)), there is only a modest difference between good and poor outcome at shorter (10–40 microns) length scales. Thus, the differences in $CD8^+$ T cell distribution between good and poor clinical outcomes are not simply attributable to differences in the architecture of cancer cell islands or stroma.

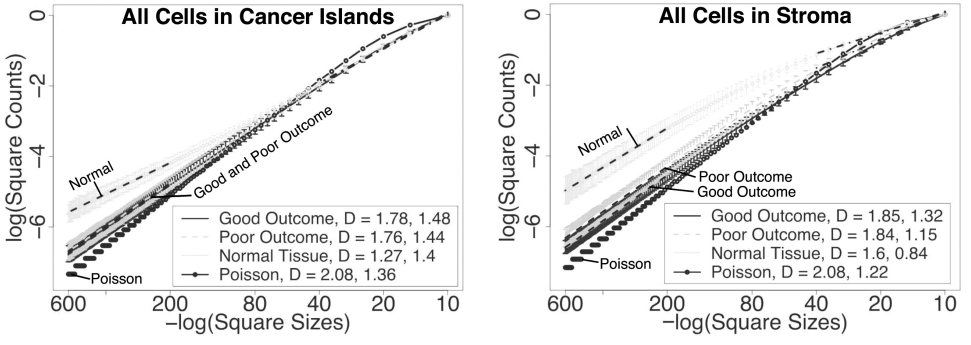

(a) (b)

Fig. 6. Log–log plot of the number of squares with at least one cell (of any type) that is in (a) a cancer cell island or epithelial tissue or (b) in the stroma versus the inverse box size in microns. (a) At long length scales (200–600 microns on the left side of plot), the mean fractal dimension x (slope) is 1.78 for good outcome (dark, solid), 1.76 for poor outcome (light, dashed), 1.27 for normal tissue (light, solid) and 2.08 for Poisson (black). The p-value for good versus poor outcome is 0.57 for long length scales. At short length scales (10–40 microns), the mean fractal dimension x (slope) is 1.48 for good outcome (dark, solid), 1.44 for poor outcome (light, dashed), 1.4 for normal tissue (light, solid) and 1.36 for Poisson (black). The p-value for good versus poor outcome is 0.49 at short length scales. (b) At long length scales (200–600 microns on the left side of plot), the mean fractal dimension x (slope) is 1.85 for good outcome (dark, solid), 1.84 for poor outcome (light, dashed), 1.6 for normal tissue (light, solid) and 2.08 for Poisson (black). The p-value for good versus poor outcome is 0.64 for long length scales. At short length scales (10–40 microns), the mean fractal dimension x (slope) is 1.32 for good outcome (dark, solid), 1.15 for poor outcome (light, dashed), 0.84 for normal tissue (light, solid) and 1.22 for Poisson (black). The p-value for good versus poor outcome is 0.013 for short length scales. Black dashed lines show the least squares linear regression fit at long and short length scales. Because different images had different numbers of squares with tissue (cells of any type), for each image, we normalized the number $n(L)$ of boxes with 1's by the total number $N(L)$ of boxes with cells in computing the fractal dimension. Thus, the y-axis values are negative. The error bars correspond to 95% confidence intervals.

Table 2. *P*-values and ROC AUC of cell density, fractal dimension (Frac Dim), fractal dimension difference, and the area under the occupancy curves (Occupancy AUC). The cell type is either $CD8^+$ T cells or all types of cells (All). The location is everywhere (All Tissue), cancer cell islands (Cancer), or Stroma. Long length scales correspond to 200–600 microns, short length scales correspond to 10–40 microns and all length scales correspond to 10–600 microns. "Mean Good" and "Mean Poor" are the mean values of the quantity averaged over the patients with good or poor clinical outcomes, respectively. The density is given in units of number of cells per square cm. The *p*-value corresponds to the null hypothesis that there is no difference in the quantity between good and poor clinical outcome. ROC AUC is the Receiver Operating Characteristic Area Under the Curve.

Quantity	Cell type	Location	Length scales	Mean good	Mean poor	*p*-value	ROC AUC
Cell Density	$CD8^+$	All Tissue		44,500	20,500	7.4×10^{-4}	0.79
Cell Density	$CD8^+$	Cancer		14,500	1830	0.0012	0.89
Cell Density	$CD8^+$	Stroma		40,200	21,300	0.021	0.79
Frac Dim	$CD8^+$	All Tissue	Long	1.7	1.5	2.8×10^{-4}	0.83
Frac Dim	$CD8^+$	All Tissue	Short	0.47	0.38	0.09	0.69
Frac Dim Difference	$CD8^+$	All Tissue		1.3	1.1	5.5×10^{-3}	0.78
Frac Dim	$CD8^+$	Cancer	Long	1.4	0.73	1.1×10^{-5}	0.89
Frac Dim	$CD8^+$	Cancer	Short	0.19	0.10	0.014	0.73
Frac Dim Difference	$CD8^+$	Cancer		1.2	0.62	1.5×10^{-5}	0.88
Frac Dim	$CD8^+$	Stroma	Long	1.7	1.4	0.0011	0.81
Frac Dim	$CD8^+$	Stroma	Short	0.49	0.40	0.066	0.69
Frac Dim Difference	$CD8^+$	Stroma		1.2	0.99	0.023	0.72
Frac Dim (thinned)	$CD8^+$	All Tissue	Long	0.85	0.90	0.41	0.57
Frac Dim (thinned)	$CD8^+$	All Tissue	Short	0.018	0.072	0.035	0.73
Frac Dim Difference (thinned)	$CD8^+$	All Tissue		0.83	0.83	0.98	0.47
Frac Dim	All	Cancer	Long	1.8	1.8	0.57	0.57
Frac Dim	All	Cancer	Short	1.5	1.4	0.49	0.61
Frac Dim	All	Stroma	Long	1.9	1.8	0.64	0.58
Frac Dim	All	Stroma	Short	1.3	1.2	0.013	0.73
Occupancy AUC	$CD8^+$	All Tissue	All	95.6	74.0	1.7×10^{-4}	0.85
Occupancy AUC	$CD8^+$	Cancer	All	65.4	29.8	1.4×10^{-5}	0.90
Occupancy AUC	$CD8^+$	Stroma	All	87.5	68.5	0.0011	0.83
Occupancy AUC (thinned)	$CD8^+$	All Tissue	All	39.5	35.5	0.28	0.64
Occupancy AUC (thinned)	$CD8^+$	Cancer	All	13.6	5.9	0.024	0.72
Occupancy AUC (thinned)	$CD8^+$	Stroma	All	58.4	54.7	0.33	0.69

Clinical significance of the occupancy, fractal dimension, and FD difference of CD8$^+$ T cells is comparable to that of CD8$^+$ T cell density.

Does the spatial distribution of CD8$^+$ T cells (as reflected in the occupancy AUC, fractal dimension and FD difference) differentiate between good and poor clinical outcome as well as that of cell density? Table 2 shows the p-values and ROC AUC of the occupancy, fractal dimension and FD difference of CD8$^+$ T cells in the various contexts described above. We compare these to the cell density (calculated by dividing the number of cells by the area) as well as to the fractal dimension of all types of cells in either the stroma or cancer cell islands. We see that in cancer cell islands and in all tissue, the clinical significance (as reflected in the p-values and ROC AUC) of the fractal dimension and FD difference of CD8$^+$ T cells at long length scales are comparable to that of CD8$^+$ T cell density, as is the area under the occupancy curves. Furthermore, for thinned CD8$^+$ T cells, the area under the occupancy curve in cancer cell islands and the fractal dimension (at short length scales) in all tissue has a small p-value, demonstrating that it is not just T cell density, but also the spatial distribution of T cells that matters clinically.

We investigated whether the clinical difference between good and poor outcome would increase by combining the CD8$^+$ T cell density and the fractal dimension of CD8$^+$ T cells. We tried various combinations of pairs where one member of the pair is CD8$^+$ T cell density and the other member is the CD8$^+$ T cell fractal dimension (all tissue, cancer cell islands, long and short length scales, thinned and un-thinned). We do not find any significant improvement in the p-values or ROC AUC, indicating that the CD8$^+$ T cell density is correlated with the CD8$^+$ T cell fractal dimension. We have confirmed this explicitly and find that the Pearson correlation coefficient (r) between the density and CD8$^+$ T cell fractal dimension varies between 0.5 and 0.9, depending on the length scales for the fractal dimension and on whether the cells are in all tissue, cancer cell islands or stroma. As expected, there is little correlation between cell density and the thinned fractal dimension.

5. Discussion

In this paper, we have presented new techniques to characterize the spatial arrangements of cells (points in space). These include occupancy and novel applications of fractal dimensions that we used to quantify the spatial distribution of cells rather than morphology. Our results indicate that the spatial distribution of the CD8$^+$ T cells as reflected in their fractal dimension at short length scales is different between good and poor clinical outcomes, even if the cell density of various samples is normalized, i.e., made to be the same. In particular, the FD difference indicates that the CD8$^+$ T cells are more spatially dispersed in good outcome compared to poor outcome. This implies that the actual spatial distribution, and not just the density of CD8$^+$ T cells, matters clinically.

Our results raise the following questions: (1) Why is the spatial distribution of T cells fractal? (2) What picks out the intermediate length scale on the order of 100

microns where the fractal dimension changes between short and long length scales? (3) Why are the fractal dimension and occupancies of $CD8^+$ T cells different between good and poor clinical outcomes? (4) Why is the spatial distribution of $CD8^+$ T cells in excised tumor tissue correlated with whether cancer recurs? Our discussion of these questions follows:

(1) Why is the spatial distribution of T cells fractal? The self-similarity of the spatial distribution of $CD8^+$ T cells is reflected in their fractal dimension at short (10–40 microns) and long (200–600 microns) length scales. We speculate that this pattern may arise from the branching trajectories of the T cells as they patrol the tissue.[1,2] Branching structures such as trees and plant roots are self-similar, and hence, fractal, because they look the same over a range of length scales, i.e., over a range of magnifications. It may be that the paths followed by $CD8^+$ T cells have a branching structure because the T cells go around physical obstacles of various sizes such as other cells, blood vessels, and collagen fibers. Regions dense with collagen fibers can impede the motion of T cells.[31,32] In addition, T cells are known to travel along the outside of blood vessels[33] and loose collagen fibers[31,32] which can have a branching architecture.

(2) What picks out the length scale on the order of 100 microns where the fractal dimension changes between short and long length scales? It may be related to the fact that $CD8^+$ T cells tend to congregate around the outside of cancer cell islands which are typically hundreds of microns in size. A hundred microns is also comparable to the diffusion length of oxygen.[34–37]

(3) Why are the fractal dimension, FD difference and occupancies of $CD8^+$ T cells different between good and poor clinical outcomes? As we have seen, some of this is the result of the difference in $CD8^+$ T cell densities found in tumor tissue from good and poor outcome patients. But even after we correct for cell density, there is still a statistically significant difference between good and poor outcome. The reason for this is not clear. It appears to be related to the $CD8^+$ T cells being more spread out spatially (fractal dimension closer to 2) in good outcome compared to poor outcome. As we reduce the density by thinning the number of cells, the fractal dimension of the cells that are spread out will approach zero which is appropriate for individual points.

    The more fundamental question is what determines the spatial distribution of $CD8^+$ T cells? Why do they go where they do? The difference in spatial distribution may reflect the difference in the spatial topography (obstacles) of the tumor microenvironment. One way to check this would be to look at the spatial distribution of other motile cell types. Another possibility is that the $CD8^+$ T cells in good outcome patients are more responsive to cytokines and more successful in finding their cognate antigen in the tumor microenvironment.

(4) Why is the spatial distribution of $CD8^+$ T cells in excised tumor tissue correlated with whether cancer recurs? It is well known that the density of T cells in excised tumor tissue can be used as a prognostic indicator.[6,7] We have found that the

spatial distribution as reflected in the fractal dimension and FD difference of $CD8^+$ T cells can also be associated with clinical outcome comparable in accuracy to cell density. The spatial distribution and density of T cells may be indicative of the responsiveness of the immune system to cancer. However, it is not understood why the spatial distribution and density of T cells in resected tumor tissue is associated with clinical outcome several years after the excision.

References

1. J. C. Wortman *et al.*, *bioRxiv* (2019). Available at: https://doi.org/10.1101/678607.
2. C. C. Yu *et al.*, arXiv:1911.11846 [physics.bio-ph] (2019).
3. W. H. Fridman, F. Pages, C. Sautes-Fridman and J. Galon, *Nat. Rev. Cancer.* **12**(4), 298 (2012). doi: 10.1038/nrc3245. PubMed PMID: 22419253.
4. B. Mlecnik *et al.*, *J. Clin. Oncol.* **29**(6), 610 (2011), doi: 10.1200/JCO.2010.30.5425. PubMed PMID: 21245428.
5. H. Angell and J. Galon, *Curr. Opin. Immunol.* **25**(2), 261 (2013), doi: 10.1016/j.coi.2013.03.004. PubMed PMID: 23579076.
6. A. Gabrielson *et al.*, *Cancer Immunol. Res.* **4**(5), 419 (2016), doi: 10.1158/2326-6066.CIR-15-0110. PubMed PMID: 26968206; PubMed Central PMCID: PMCPMC5303359.
7. P. C. Tumeh *et al.*, *Nature* **515**(7528), 568 (2014), doi: 10.1038/nature13954. PubMed PMID: 25428505; PubMed Central PMCID: PMCPMC4246418.
8. J. Saltz *et al.*, *Cell Rep.* **23**(1), 181 (2018), doi: 10.1016/j.celrep.2018.03.086. PubMed PMID: 29617659; PubMed Central PMCID: PMCPMC5943714.
9. A. Berthel *et al.*, *Oncoimmunology.* **6**(3), e1286436 (2017), doi: 10.1080/2162402X.2017.1286436. PubMed PMID: 28405518; PubMed Central PMCID: PMCPMC5384380.
10. Y. Yuan, *Cold Spring Harb. Perspect. Med.* **6**(8), 1 (2016), doi: 10.1101/cshperspect.a026583. PubMed PMID: 27481837; PubMed Central PMCID: PMCPMC4968167.
11. C. C. Maley, K. Koelble, R. Natrajan, A. Aktipis and Y. Yuan, *Breast Cancer Res.* **17**(1), 131 (2015), doi: 10.1186/s13058-015-0638-4. PubMed PMID: 26395345; PubMed Central PMCID: PMCPMC4579663.
12. A. Getis and J. K. Ord, *Geographical Analysis.* **24**(3), 189 (1992), doi: 10.1111/j.1538-4632.1992.tb00261.x. PubMed PMID: WOS:A1992JF93400001.
13. S. Nawaz, A. Heindl, K. Koelble and Y. Yuan, *Mod. Pathol.* **28**(6), 766 (2015), doi: 10.1038/modpathol.2015.37. PubMed PMID: 25720324.
14. Y. Yuan, *J. R. Soc. Interface.* **12**(103), 20141153 (2015), doi: 10.1098/rsif.2014.1153. PubMed PMID: 25505134; PubMed Central PMCID: PMCPMC4305416.
15. The Cancer Genome Atlas Program [Internet]. Available at: https://www.cancer.gov/about-nci/organization/ccg/research/structural-genomics/tcga.
16. R. Natrajan, H. Sailem, F. K. Mardakheh, M. Arias Garcia, C. J. Tape, M. Dowsett *et al.*, *PLoS Med.* **13**(2), e1001961 (2016), doi: 10.1371/journal.pmed.1001961. PubMed PMID: 26881778; PubMed Central PMCID: PMCPMC4755617.
17. B. B. Mandelbrot, *The Fractal Geometry of Nature* (W. H. Freeman and Co., New York, 1983).
18. M. Tambasco, M. Eliasziw and A. M. Magliocco, *J. Transl. Med.* **8**, 140 (2010), doi: 10.1186/1479-5876-8-140. PubMed PMID: 21194459; PubMed Central PMCID: PMCPMC3024250.
19. V. Velanovich, *Breast Cancer Res. Treat.* **49**(3), 245 (1998). PubMed PMID: 9776508.

20. A. Chan and J. A. Tuszynski, *R. Soc. Open Sci.* **3**(12), 160558 (2016), doi: 10.1098/rsos.160558. PubMed PMID: 28083100; PubMed Central PMCID: PMCPMC5210682.
21. J. W. Baish and R. K. Jain, *Nat. Med.* **4**(9), 984 (1998), doi: 10.1038/1952. PubMed PMID: 9734370.
22. J. W. Baish and R. K. Jain, *Cancer Res.* **60**(14), 3683 (2000). PubMed PMID: 10919633.
23. F. E. Lennon, G. C. Cianci, R. Kanteti, J. J. Riehm, Q. Arif, V. A. Poroyko *et al.*, *Sci. Rep.* **6**, 24578 (2016), doi: 10.1038/srep24578. PubMed PMID: 27080907; PubMed Central PMCID: PMCPMC4832330.
24. P. Bose, N. T. Brockton, K. Guggisberg, S. C. Nakoneshny, E. Kornaga, A. C. Klimowicz *et al.*, *BMC Cancer.* **15**, 409 (2015), doi: 10.1186/s12885-015-1380-0. PubMed PMID: 25976920; PubMed Central PMCID: PMCPMC4435912.
25. P. Waliszewski, F. Wagenlehner, S. Gattenlohner and W. Weidner, *Prostate.* **75**(4), 399 (2015), doi: 10.1002/pros.22926. PubMed PMID: WOS:000347811800007.
26. P. Waliszewski, *Front Physiol.* **7**, 34 (2016), doi: 10.3389/fphys.2016.00034. PubMed PMID: 26903883; PubMed Central PMCID: PMCPMC4749702.
27. H.-O. Peitgen, H. Jürgens and D. Saupe, *Chaos and Fractals: New Frontiers of Science* (Springer-Verlag, New York, 1992).
28. A. Baddeley and R. Turner, *J. Statist. Softw.* **12**(6), 1 (2005).
29. G. Pau, F. Fuchs, O. Sklyar, M. Boutros and W. Huber, *Bioinformatics.* **26**(7), 979 (2010).
30. J. A. Swets, *Science* **240**(4857), 1285 (1988).
31. H. Bougherara *et al.*, *Front Immunol.* **6**, 500 (2015), doi: 10.3389/fimmu.2015.00500. PubMed PMID: 26528284; PubMed Central PMCID: PMCPMC4600956.
32. H. Salmon *et al.*, *J. Clin. Invest.* **122**(3), 899 (2012), doi: 10.1172/JCI45817. PubMed PMID: 22293174; PubMed Central PMCID: PMCPMC3287213.
33. A. Boissonnas, L. Fetler, I. S. Zeelenberg, S. Hugues and S. Amigorena, *J. Exp. Med.* **204**(2), 345 (2007), doi: 10.1084/jem.20061890. PubMed PMID: 17261634; PubMed Central PMCID: PMCPMC2118741.
34. J. M. Brown and A. J. Giaccia, *Cancer Res.* **58**(7), 1408 (1998). PubMed PMID: 9537241.
35. I. J. Fidler, S. Yano, R. D. Zhang, T. Fujimaki and C. D. Bucana, *Lancet Oncol.* **3**(1), 53 (2002). Epub 2002/03/22. PubMed PMID: 11905606.
36. I. F. Tannock, *Br. J. Cancer.* **22**(2), 258 (1968). PubMed PMID: 5660132; PubMed Central PMCID: PMCPMC2008239.
37. L. H. Gray, A. D. Conger, M. Ebert, S. Hornsey and O. C. Scott, *Br. J. Radiol.* **26**(312), 638 (1953). Epub 1953/12/01. PubMed PMID: 13106296.